JACS
JOURNAL OF THE AMERICAN CHEMICAL SOCIETY
pubs.acs.org/JACS

Article

Anomalous Saturation of CO Adsorption at 26% on Cu(111) Governed by Nanometer-Scale Substrate-Mediated Interactions

Pengcheng Chen,[#] Dingxin Fan,[#] Annabella Selloni, Jianqing Fan, and Nan Yao*

Cite This: J. Am. Chem. Soc. 2026, 148, 360−367

Read Online

ACCESS | Metrics & More | Article Recommendations | Supporting Information

ABSTRACT: CO adsorption on metal surfaces is a process of fundamental importance in surface science and heterogeneous catalysis. Despite its apparent simplicity, its understanding has often posed a challenge to conventional models. Using scanning probe microscopy (SPM), we have observed that CO adsorption on Cu(111) saturates at ∼26%, significantly below the anticipated 33% for the canonical $\sqrt{3} \times \sqrt{3}$/R30° structure. This anomalous saturation persists across a wide range of dosing amounts and deposition temperatures, indicating an intrinsic thermodynamic constraint rather than kinetic trapping. Statistical analysis of the SPM images reveals a long-range adsorbate interaction radius of ∼5.3 nm that governs the two-dimensional distribution of CO molecules. This nanometer-scale, substrate-mediated indirect interaction induces spatial correlations that suppress higher coverage. First-principles calculations show that increased coverage leads to confinement of Cu(111) surface-state electrons, with overlapping elastic strain fields, both of which reduce CO binding energy. These long-range interactions collectively enforce a self-limiting adsorbate density. Our findings establish that substrate-mediated forces can govern adsorbate arrangements well beyond nearest-neighbor scales. CO/Cu(111) provides a model system in which such effects can be observed directly, serving as a testbed for established theories of adsorption and substrate-mediated interactions.

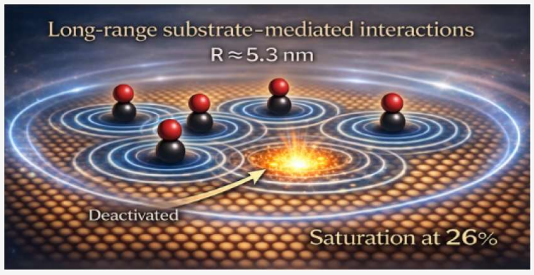

1. INTRODUCTION

Adsorption of atoms and molecules on solid surfaces governs a wide range of physical and chemical phenomena, from heterogeneous catalysis and surface reactions to the design of nanoscale devices.[1] Decades of theoretical and experimental efforts have produced increasingly refined models of surface adsorption,[2,3] showing that adsorbates can perturb the electronic and elastic environment of a surface in ways that propagate over significant distances. In particular, much attention has been focused on molecular adsorption on noble metal surfaces such as Cu, where the presence of a 2D electron gas associated with Shockley-type surface states can mediate long-range oscillatory interactions between adsorbates.[4,5] Simultaneously, local lattice distortions induced by adsorption can couple across nanometers via elastic strain fields.[6,7] Although substrate-mediated interactions between adsorbates were theoretically predicted[6] and experimentally observed to influence adsorbate distributions,[8] their role in globally dictating surface adsorption and fundamentally limiting the achievable coverage have remained unexplored.

Carbon monoxide (CO) is a chemically stable molecule that interacts moderately with the lowest energy and most compact (111) surface of copper, making the CO/Cu(111) system particularly suited for isolating long-range and substrate-mediated effects that may be obscured in more strongly bound systems. In this work, we investigate CO adsorption on Cu(111) and uncover an unexpected phenomenon: when saturated with CO, the surface consistently reaches a coverage of ∼26%, well below the anticipated 33% for a close-packed $\sqrt{3} \times \sqrt{3}$/R30° adsorption structure[9] (Figure 1A). This result is robust across a range of deposition temperatures and persists even under substantial CO overdosing. The data indicate that this low coverage is not due to kinetic trapping or surface defects but instead reflects an intrinsic thermodynamic limit set by long-range interactions. However, the anomalous saturation of CO is system-specific and condition-dependent, as illustrated by previous work on other similar interface systems.[10−14] Under low-temperature and ultrahigh-vacuum conditions, the Cu(111) substrate remains atomically flat, allowing us to isolate the effect of long-range adsorbate interactions on the observed self-limited coverage. In contrast, under more reactive environments, for example at room temperature and near-ambient pressures, CO adsorption has been shown to activate the Cu(111) surface through Cu adatom formation and nanocluster reconstruction.[15]

Using atomic-resolution scanning probe microscopy (SPM), we systematically characterize the spatial distribution of

Received: August 7, 2025
Revised: December 17, 2025
Accepted: December 22, 2025
Published: December 26, 2025

https://doi.org/10.1021/jacs.5c13663
J. Am. Chem. Soc. 2026, 148, 360−367

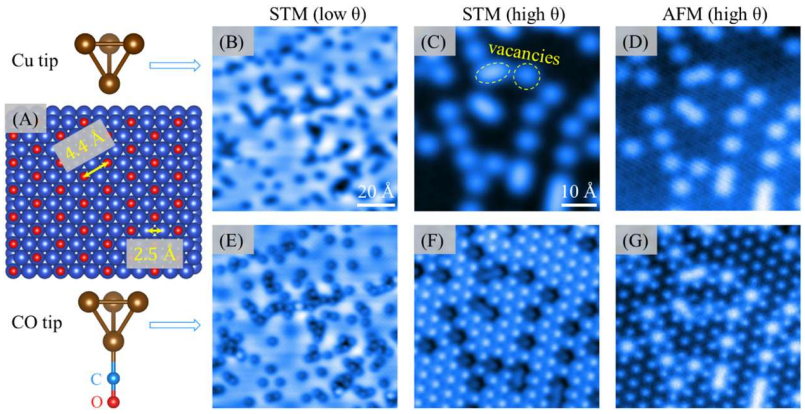

Figure 1. CO distribution on a Cu(111) surface. (A) Schematic of the $\sqrt{3} \times \sqrt{3}$/R30° adsorption structure, where the separation distance between nearest neighbor COs and Cu atoms are 4.4 and 2.5 Å, respectively. (B, C, E, F) are STM images (set point: V_{sample} = + 100 mV, I = 100 pA), and (D, G) are AFM images showing CO molecules on a Cu(111) surface using Cu (top panel) and CO (bottom panel) terminated tips at low (B, E) and high/saturated (C, D, F, G) coverages. (B, E) show the same area, and (C, D, F, G) show another identical region at the same magnification. The contrast in (G) can be inverted by decreasing the tip height (Figure S1).

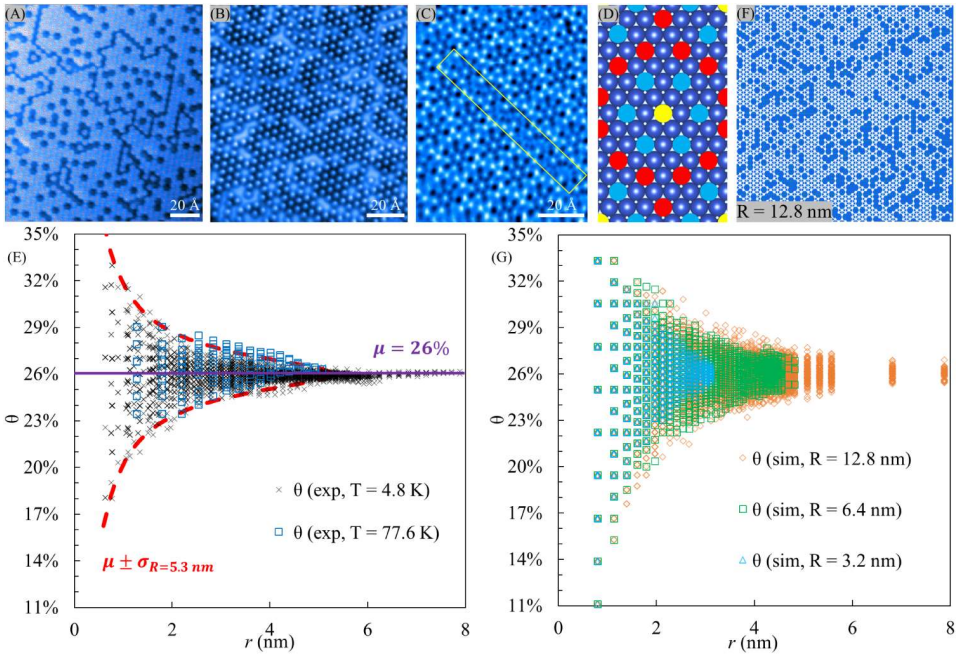

Figure 2. Statistical analysis. (A) Large-scale STM and (B) AFM images of two random distributions of adsorbed COs on a Cu(111) surface, obtained using CO tips; the separation distance between nearest neighbor COs is 4.4 Å. The CO molecules, deposited at 4.8 K, are represented by small red circles in (A). (C) AFM image of an ordered phase of adsorbed CO formed at 77.6 K; the yellow box marks a lattice mismatch area. (D) Schematic of the unit cell of the ordered CO phase in (C). The yellow, blue, and red solid circles indicate COs in different adsorption environments, characterized by different numbers of nearest and next-nearest neighbor COs. The ideal coverage for this phase is 26.5%. See Figure S4 in Supporting Information for other patterns formed at 77.6 K. (E) Experimental CO coverage data as a function of sampled image size, *r*. Here, μ represents the mean of all experimental data (26%), and σ_R represents the standard deviation for a CO confinement/interaction radius *R*. The latter is determined to be 5.3 nm, assuming a hypergeometric statistical distribution. The red dashed curves show the statistical solution, $\mu \pm \sigma_{R=5.3nm}$. (F) CO distribution on a Cu(111) surface from Monte Carlo simulations; the white solid circles represent CO molecules. The coverage is $\theta_{sim} = \frac{n_{co}}{n_{cu}} = \frac{2,397}{9,216} = 26.0\%$. (G) Simulated CO coverage data as a function of sampled image size, r, obtained using R = 12.8 (brown), 6.4 (green), and 3.2 (blue) nm.

adsorbates and apply statistical analysis to extract an effective interaction range. We find that each CO molecule influences adsorption within a radius of ~5.3 nm, a length scale far exceeding that of chemical bonding or the short-range, few-neighbor interactions assumed in early adsorption models.[3] First-principles calculations further reveal that increased CO coverage leads to a confinement of surface-state electrons and a downward shift of the Cu d-band center, both of which reduce the CO binding energy.[16] Elastic strain also builds up at high coverage, compounding the energetic penalty. These effects together explain why further adsorption becomes increasingly unfavorable as the system approaches 26% coverage. Our work provides direct evidence that substrate-mediated interactions, rather than steric saturation or surface poisoning, dictate the

https://doi.org/10.1021/jacs.5c13663
J. Am. Chem. Soc. 2026, 148, 360−367

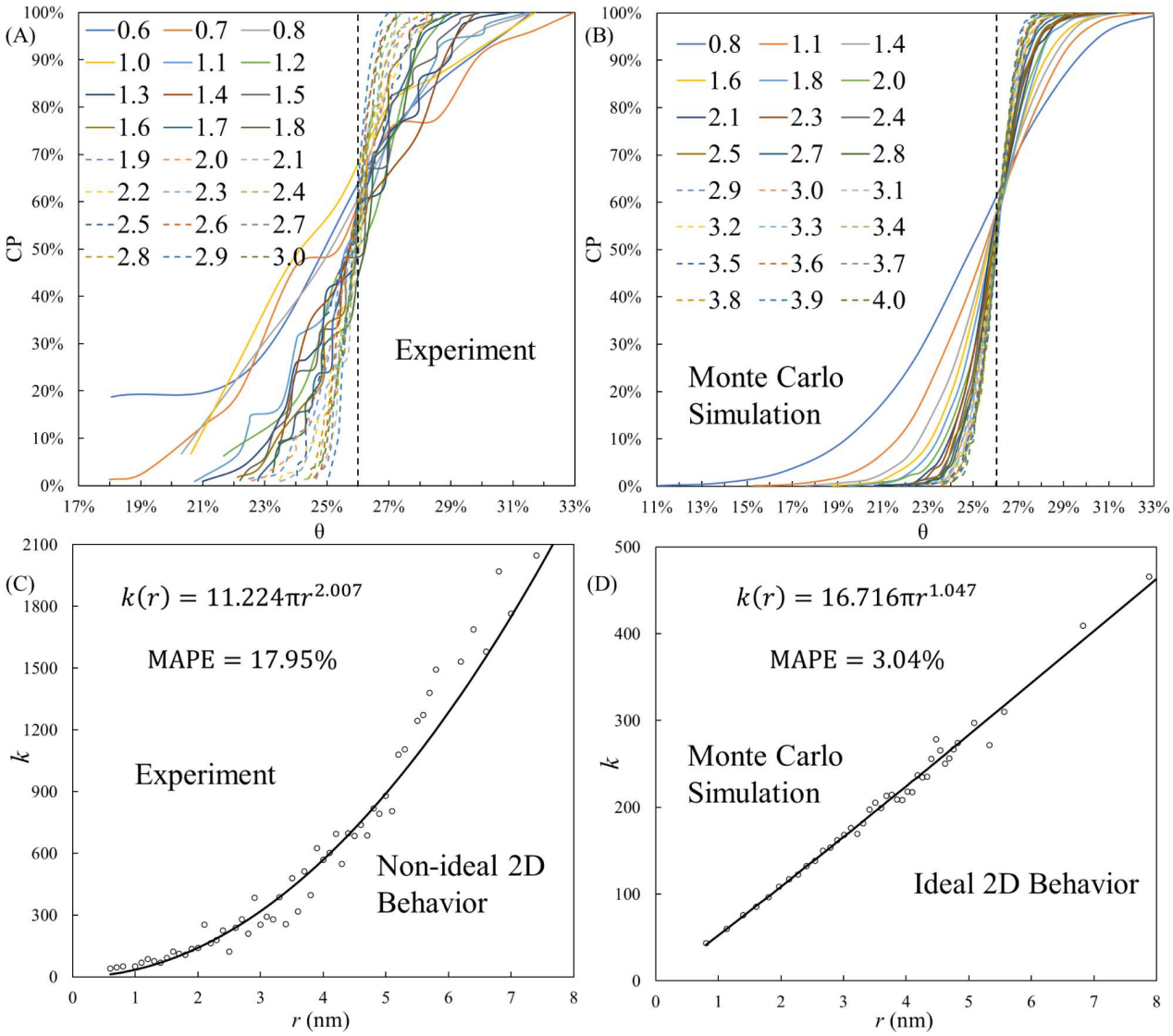

Figure 3. Analysis of the behavior of the CO distribution. (A) Experimental and (B) simulated (R = 12.8 nm) cumulative probability (CP) as functions of θ for different image radii (unit: nm). The CP is taken of the form $\mathrm{CP}(\theta) = \frac{1}{1+e^{-k(r)(\theta-L(r))}}$, where both $k(r)$ and $L(r)$ are functions of the image radius r. $k(r)$ represents the stiffness of the curve, and $L(r)$ is the inflection point, which can also be interpreted as the most likely observed θ for an image of size r. (C) and (D) are the fitted $k(r)$ curves for (A) and (B), corresponding to experimental nonideal 2D behavior and simulated ideal 2D behavior, respectively. The calculated Mean Absolute Percentage Errors (MAPE) for (C) and (D) are 17.95% and 3.04% (<20%), respectively, demonstrating the reliability of our fittings.[23]

global arrangement of adsorbates and impose an intrinsic limit on adsorption coverage.

2. RESULTS AND DISCUSSION

2.1. Experimental Characterization and Image Interpretation. We employed atomic-resolution SPM imaging techniques (scanning tunneling microscopy (STM) and atomic force microscopy (AFM)) to examine the distribution of CO molecules adsorbed on Cu(111) surfaces using both Cu (Figure 1B–D) and CO (Figure 1E–G) tips[17] (see Supporting Information Sections 1.1 and 1.2 for details). CO deposition was carried out at two different temperatures, 4.8 and 77.6 K, while SPM measurements were always performed at 4.8 K under ultrahigh vacuum (UHV) conditions (10^{-11} Torr).

COs appear as dark circular spots in STM images with a Cu tip (Figure 1B and C), whereas each bright circular spot corresponds to a CO molecule when using a CO tip (Figure 1E,F) since Cu is an *s*-wave tip and CO is a *p*-wave tip.[18] Figure 1C,F shows numerous large circular spots that remain present even when the amount of CO introduced into the chamber greatly exceeds the expected saturation level (these conditions are used as default throughout all subsequent experiments). Further images of the same region, obtained using AFM (Figure 1D and G), support the idea that the bright circular spots represent CO vacancies. Moreover, we used a CO tip to push the surface COs toward vacancy-like sites (see Figure S1 for details of this procedure). These manipulation experiments confirmed that the vacancy-like sites indeed correspond to point defects, specifically point vacancies. These results demonstrate that CO adsorption on Cu(111) remains incomplete even under oversaturation conditions, with the saturation coverage θ_{sat} less than the canonical 33%.

https://doi.org/10.1021/jacs.5c13663
J. Am. Chem. Soc. 2026, 148, 360−367

Figure 2A,B display two large-scale SPM images of randomly distributed CO molecules deposited at 4.8 K under oversaturation conditions. Local disorder of the CO layer originates from the coexistence of different types of line vacancies with distinct CO−CO separations (see Figure S2C and D). We employed a peak detection method (see Supporting Information Section 2.1) to identify the COs in the images. In Figure 2A, we identified n_{CO} = 943 adsorbed COs (red circles) in an image of size ∼ 20,365 Å^2, corresponding to 3,609 surface Cu atoms (n_{Cu}). Therefore, the CO coverage was calculated as $\theta = \frac{n_{CO}}{n_{Cu}} = \frac{943}{3,609} \cong 26\%$ Similar to Figure 1, despite the excess of CO, all these images reveal a significant presence of CO vacancies. In addition to point vacancies, the images also contain line-type vacancies. These correspond to the boundaries between lattice mismatched domains of adsorbed COs, which could further lower the saturation coverage θ because their formation "deactivates" a large number of surface sites for CO adsorption (Figure S2). Our DFT calculations indicate a slight energetic preference for line vacancy formation compared to point vacancy when θ > 20% (Figure S3), but this alone cannot account for the large number of point vacancies observed.

At 77.6 K, CO molecules organize into a variety of ordered domains, all exhibiting similar overall coverages. Figure 2C displays one representative pattern, with an ideal coverage of 26.5% derived from its unit cell geometry (Figure 2D). Other patterns are presented in Figure S4. The similarity between the observed ∼26% saturation coverage and the fraction of empty space in face-centered cubic metals is intriguing and may deserve further study.

2.2. Statistical Analysis. We analyzed over 3,400 SPM images obtained from different samples, including large-scale images and their partitioned "sub-images" (see Figure 2E for the statistical data). Our results show that as the image radius (r) increases, θ converges to the sample mean (μ = 26%). Moreover, the θ distribution at 77.6 K is nearly identical to that observed at 4.8 K, and its average is even slightly higher. This behavior contrasts with the typical expectation where a higher temperature should enhance adsorbate mobility, weaken the Cu-CO binding strength, and thus lower the saturation coverage. This suggests that the system can be stabilized by forming ordered patterns.

To rationalize these experimental findings, we simulated the CO/Cu(111) system using a Monte Carlo approach (see Supporting Information Section 2.2; the code is available on GitHub), where the adsorbed COs are assumed to "see" each other over a certain interaction radius, R. Figure 2F exemplifies a simulated image with R = 12.8 nm, containing 2,397 COs and 9,216 Cu atoms. By analyzing over 30,000 simulated images and varying R from 12.8 to 3.2 nm, we found that the behavior of the simulated coverage could reproduce the experimental observations (Figure 2E). This suggests an experimental boundary/limit to how far CO molecules influence each other's adsorption. By comparing the convergence rates of the experimental and simulated data (for r > 2 nm) in Figure 2E,G, we could also infer that the experimental R is likely to lie between 3.2 and 6.4 nm.

To determine the experimental R more precisely, we assumed that our system obeys a hypergeometric statistical distribution because we repeatedly sampled subimages with radii r_i from larger images without replacement.[19,20] The corresponding standard deviation, σ_{r_i}, was calculated using

$$\sigma_{r_i} = \sqrt{\frac{\mu(1-\mu)}{n_{Cu_i}}} \times \sqrt{\frac{N_{Cu} - n_{Cu_i}}{N_{Cu} - 1}} \quad (1)$$

where μ is the sample mean, n_{Cu_i} is the number of surface Cu atoms in a sampled image from the ith experiment, N_{Cu} is the total number of surface Cu atoms within the area of radius R. We solved for R by minimizing the random stochastic error in a first-order approximation (See Supporting Information Section 2.3) while varying N_{Cu} from 570 (corresponding to R = 3.2 nm) to 2,280 (corresponding to R = 6.4 nm). With this procedure, we obtained R = 5.3 nm, a value of the same magnitude as the radius of surface long-range interactions identified in previous work.[8,21,22] The red dashed curves in Figure 2E indicate the range of possible coverages $\theta(r)$ for a given image size, statistically solved with a confidence interval of 68%.

We found that the experimental data exhibited significantly faster convergence than our simulated data for small image sizes (r < 2 nm). This suggests that the apparent randomness in the experimental distribution of vacancies is constrained by a local self-regulating mechanism, which helps to maintain a stable coverage and avoids extreme scenarios, leading to faster convergence in the experiments.

Figure 3A,B shows the experimental and the simulated cumulative probability (CP) as a function of θ for different image radii. To quantify the behavior of the distribution, we represented the CP as a Sigmoid function:

$$\mathrm{CP}(\theta) = \frac{1}{1 + e^{-k(r)(\theta - L(r))}} \quad (2)$$

Here r is the radius of the measured image, $k(r)$ represents the degree of concentration of data points in the data set, $L(r)$ represents the most likely value of θ for an image of size r. Our experimental data show that $L(r)$ is a constant, 26%. Based on the plotted $k(r)$ curves, we assumed that $k(r)$ follows a power-law type function, $k(r) = ar^b$. By least-squares fitting, we obtained $a_{exp} = 11.224\pi$, $b_{exp} = 2.007 \cong 2$ for the experimental CP, and $a_{sim} = 16.716\pi$, $b_{sim} = 1.047 \cong 1$ for the simulated one (see Figure 3C,D; details of the fitting are available on GitHub). These fitted values allow us to calculate the range of possible outcomes when measuring θ. The confidence level (n %) can be calculated using

$$n\% = \frac{2\ln\left(\frac{100+n}{100-n}\right)}{k(r)} \quad (3)$$

Thus, if we wish to determine θ from a random experimental image with a radius of 4 nm, there is a 95% probability that the results will fall within $26\% \pm \frac{2\ln\left(\frac{100+95}{100-95}\right)}{11.224 \times \pi \times 4^{2.007}} \rightarrow (24.7\%,\ 27.3\%)$.

Interestingly, our experimental data show a quadratic dependence of $k(r)$ on r (Figure 3C), while the simulation data show a linear relationship (Figure 3D). The fitted exponent values (2 and 1) suggest that the experimental data deviates from the ideal 2D behavior, as determined by Monte Carlo simulations. The origin of this deviation will be discussed in the following.

2.3. Adsorbate−Adsorbate Electronic Interaction. To study the electronic interactions between adsorbed species, we computed[24] the adsorption energy per CO, $E_{ad/CO}$, as a function of θ

https://doi.org/10.1021/jacs.5c13663
J. Am. Chem. Soc. 2026, 148, 360−367

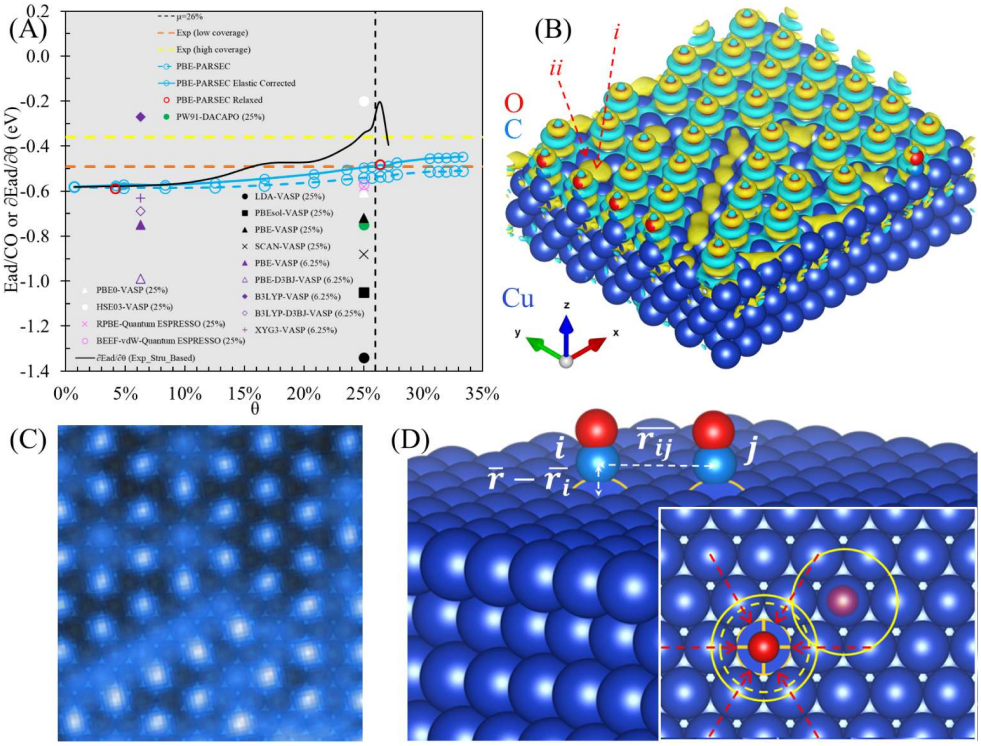

Figure 4. DFT calculations and elastic correction. (A) Calculated CO adsorption energy and its derivative with respect to θ as functions of θ. The brown and yellow dashed lines indicate the lower and upper limits of $E_{ad/CO}$ from experimental measurements. The dashed and solid curves in cyan show our calculated $E_{ad/CO}$ before and after applying the elastic correction in eq 5. The green, black, purple, white, and pink symbols denote calculated $E_{ad/CO}$ values at θ = 6.25% and 25% from ref 25, ref 26, ref 27 ref 28, and ref 29, respectively, obtained using the corresponding exchange−correlation functionals and codes. (B) Change in electron density upon CO adsorption at θ = 26.4%, (isovalue: 0.00005 $e^-/Å^3$, yellow: positive, cyan: negative.) The surface configuration used for the calculation is based on the experimental AFM image (C), overlaid on a Cu(111) model. (D) Schematic of elastic effect at a CO/Cu(111) interface for two CO molecules at a separation distance $\overline{r_{ij}}$. The adsorption height equals $\overline{r} - \overline{r_{i/j}}$. The inset shows a top view of the system where the CO on the left side is assumed to arrive at the surface first, and the transparent CO is assumed to be adsorbed next. The large yellow solid circles show the original positions of the six neighboring atoms around the binding sites, and the small yellow dashed circle and red arrows illustrate the contractive movement upon the adsorption of the first CO.

$$E_{ad/CO}(\theta) = \frac{E_{sys} - (E_{nCO} + E_{Cu(111)})}{n} \quad (4)$$

Here n is the number of adsorbed CO molecules, E_{sys} represents the total energy of the nCO/Cu(111) system (surface with n adsorbed molecules),E_{nCO} is the energy of the nCO system without a substrate and $E_{Cu(111)}$ represents the energy of the bare Cu(111), modeled using a four-layer 12 × 12 slab exposing 144 surface Cu atoms. We used eq 4 instead of taking the energy of an nCO system equal to n times the energy of a single CO molecule in the vacuum (nE_{CO}), because we found that different surface distribution patterns, Ω, of the adsorbed CO's can have slightly different values of $E_{ad/CO}$ even when their coverages are the same. To minimize such Ω dependence, we then replaced nE_{CO} with E_{nCO} (see Figure S5 for a detailed comparison).

In Figure 4A, the green,[25] black,[26] purple,[27] white,[28] and pink[29] symbols denote $E_{ad/CO}$ values (from −1.34 to −0.20 eV) at θ = 6.25% and 25% from previous theoretical calculations. Most of these exchange−correlation functionals (PW91,[30] LDA,[31] PBEsol,[32] PBE,[33] SCAN,[34] XYG3,[35] PBE0,[36] RPBE,[37] and BEEF-vdW[38]) substantially overestimated the CO−Cu binding strength compared with experimental values, which range from −0.49 eV[9],[39] at low coverage to −0.36 eV[9] at high coverage (brown and yellow dashed horizontal lines in Figure 4A), while B3LYP[40] and HSE03,[41] including a fraction of Hartree−Fock exchange, yielded slightly weaker binding. D3BJ corrections[42] were considered for PBE and B3LYP. In our large unit cell-based calculations (see Supporting Information Section 2.4 for details), the adsorption energy of CO (computed at fixed surface geometry) varies from −0.58 to −0.51 eV, with increasing θ (blue dashed curve in Figure 4A), showing a reasonable agreement with experiment.

Figure 4B shows the computed change in electron density upon adsorption, $\Delta\rho(\theta)$ (see Supporting Information Section 2.4), for a CO adsorption configuration constructed based on an experimental AFM image (Figure 4C). $\Delta\rho(\theta)$ exhibits an excess electron density, appearing as "bubbles", above vacant surface Cu atoms. The formation of such "bubbles" can be attributed to the quantum confinement of the 2D surface state electrons of Cu(111) induced by the adsorption of CO.[8] It is also noteworthy that the enhancement of electronic density at point vacancies (such as the i site) significantly surpasses that on the neighboring atoms (such as the ii site), which are "deactivated" by the adsorbed CO, in agreement with the measured STM image obtained with an s-wave Cu tip[18,43] (Figure 1C).

When a CO molecule adsorbs on a top site of a Cu(111) substrate, its 5σ orbital interacts with the 3dz^2 orbital of a Cu atom.[44,45] Our calculations show that Cu's in-plane 3d orbitals shift toward the Fermi level upon CO adsorption, while the changes of the out-of-plane orbitals are much less pronounced.

https://doi.org/10.1021/jacs.5c13663
J. Am. Chem. Soc. 2026, 148, 360−367

Moreover, the width of Cu's d band shrinks by ∼20% as θ increases from 0 to 33.3% (see Supporting Information Section 2.6 for details). This compression causes a shift toward lower energy of the d-band center, a well-known reactivity descriptor in surface chemisorption.[46] For θ > 20%, there is also an increase of the energy gap (Δ) between $3d_{z^2}$, and the in-plane orbitals (Figure S6), which makes the interaction between the CO's 5σ and the Cu's $3d_{z^2}$ orbitals less favorable. These changes in surface electronic states, together with the formation of the electron "bubbles", can weaken the strength of the Cu-CO binding.

2.4. Indirect Elastic Interaction (IEI). The IEI between adsorbed CO molecules is always repulsive for our system. As illustrated in Figure 4D, the adsorption of a CO molecule generates an overall pulling force on the nearby Cu atoms, which leads to a tightening of the lattice near this CO and an expansion away from it (indicated by the yellow dashed circles and red arrows). When a second CO molecule is adsorbed near the first one, it will also attempt to induce a tightening of the nearby lattice. However, this will be hindered by the expansion caused by the first CO, ultimately causing a repulsive force between the two CO molecules.[7,47]

In DFT calculations, the effect of IEI is generally included through structural relaxation. However, relaxing the atomic positions of a system as large as our slab model is computationally costly. Therefore, we fully relaxed the system at low (θ = 4.2%) and high (θ = 26.4%) coverages only (red circles in Figure 4A). The relaxed systems exhibit less negative adsorption energies. This is because the lattice constant is obtained from the bulk system. When constructing the surface using this lattice constant, the surface atoms experience residual stress due to the loss of coordination at the surface. Upon relaxation, the surface structure adjusts to compensate for undercoordination, an effect that is partially offset by CO adsorption through restoring coordination at the adsorption sites.[48] As a result, the decrease in E_{sys}^{rel} is smaller than the decrease in $E_{Cu(111)}^{rel}$, leading to less negative adsorption energies. To reduce the computational cost, we introduce an additional term, $E_{elastic}(\theta, \Omega)$, to account for the IEI energy between molecules at all other investigated CO coverages. To evaluate the adsorption energy per CO we thus redefine $E_{ad/CO}(\theta, \Omega)$ as

$$E_{ad/CO}(\theta, \Omega) = \frac{E_{sys}^{unrel} - (E_{nCO} + E_{Cu(111)}) + E_{elastic}(\theta, \Omega)}{n} \quad (5)$$

where E_{sys}^{unrel} is the total energy of the unrelaxed system while $E_{elastic}(\theta,\Omega)$ is calculated using a revised version of the two-adatom interaction expression[7] (see Supporting Information Section 2.7 for details).

Figure 4A shows that the elastic corrected adsorption energies (blue solid curve) agree well with the computed energies for the relaxed structures (red circles). Our calculated adsorption energy ranges from −0.58 eV at low coverage to −0.45 eV at high coverage. Although the absolute values are about 0.09 eV lower than the experimental measurements (−0.49 eV at low coverage; −0.36 at high coverage),[9,39] the coverage-dependent trend is consistent. From low to high coverage, the adsorption energy increases by 0.13 eV, indicating a progressive weakening of CO binding strength, in excellent agreement with experiment.

Additionally, we evaluated the chemical potential of adsorbed CO for several structures derived from experimental images by taking the first derivative of the adsorption energy with respect to θ (black solid curve in Figure 4A). We observed a sharp drop in the chemical potential of CO at θ = 26%, indicating a substantial change of the interface properties. This drop followed a noticeable upward bend of the curve at θ > 20%, suggesting that adsorption becomes increasingly unfavorable. This observation agrees with the observed change in electronic structure when θ reaches 20% (Figure S6), which is most likely related to the quantum confinement of the 2D surface state electrons.

3. CONCLUSIONS

CO adsorption on Cu(111) saturates at ∼26%, substantially below the anticipated 33% for the $\sqrt{3} \times \sqrt{3}$/R30° structure. This anomalous limit is robust across a significant range of dosing and temperature conditions, indicating an intrinsic thermodynamic constraint rather than kinetic hindrance. Atomic-scale imaging and statistical analysis reveal that CO molecules influence adsorption over ∼5.3 nm, far exceeding chemical bonding ranges. DFT calculations reveal that substrate-mediated electronic interactions, facilitated by elastic effects, progressively weaken CO binding with increasing coverage, thereby enforcing a collective self-limiting density. Comparable systems such as Ag(111)[12] and Pt(111)[13] have not shown a similarly pronounced manifestation of this effect, underscoring that Cu(111) serves as an ideal platform to identify the crucial role of substrate-mediated interactions in shaping interface structures beyond simple steric saturation or surface poisoning.

Although the CO adsorption configurations reported here are only stable under low-temperature and ultrahigh-vacuum conditions, the underlying mechanism of substrate-mediated collective interactions is conceptually relevant to heterogeneous catalysis, as recognized in prior model-surface studies.[49−51] The discovery that collective surface responses can globally dictate adsorption arrangements suggests broader implications for surface chemistry. Intrinsic limits on adsorbate density may critically impact catalytic performance.[52] Finally, our findings offer experimental/empirical validation of a recent theoretical prediction[53] that strong adsorbate−adsorbate interactions induce a nonlinear quadratic coverage dependence of adsorption energy, leading to self-limiting arrangements of adsorbates on surfaces.

■ ASSOCIATED CONTENT

Supporting Information

The Supporting Information is available free of charge at https://pubs.acs.org/doi/10.1021/jacs.5c13663.

Experimental methods, computational methods, GitHub repository (containing the codes used in this work and the data sheets for statistical analysis), supporting figures, and supporting references (PDF)

■ AUTHOR INFORMATION

Corresponding Author

Nan Yao − *Princeton Materials Institute, Princeton University, Princeton, New Jersey 08540, United States;* orcid.org/0000-0002-4081-1495; Email: nyao@princeton.edu

https://doi.org/10.1021/jacs.5c13663
J. Am. Chem. Soc. 2026, 148, 360−367

Authors

Pengcheng Chen − *Princeton Materials Institute, Princeton University, Princeton, New Jersey 08540, United States*

Dingxin Fan − *Princeton Materials Institute, Princeton University, Princeton, New Jersey 08540, United States;* orcid.org/0000-0001-6850-9362

Annabella Selloni − *Department of Chemistry, Princeton University, Princeton, New Jersey 08544, United States;* orcid.org/0000-0001-5896-3158

Jianqing Fan − *Department of Operations Research and Financial Engineering, Princeton University, Princeton, New Jersey 08544, United States*

Complete contact information is available at: https://pubs.acs.org/10.1021/jacs.5c13663

Author Contributions

#P.C. and D.F contributed equally to this work.

Notes

The authors declare no competing financial interest.

■ ACKNOWLEDGMENTS

This research made use of the Imaging and Analysis Center at Princeton University, which is supported in part by the Princeton Center for Complex Materials, a National Science Foundation Materials Research Science and Engineering Center (grant no. DMR-2011750), and the Texas Advanced Computing Center (TACC). We acknowledge partial support from the Evin-Catalysis Initiative Award at Princeton. We thank Prof. John P. Perdew for discussing the possibility of our system being strongly correlated and for providing insights into the DFT+*U* method. We thank Prof. Tianjian Cheng, Dr. Ziwei He, Ms. Qiaoqiao Chi, and Prof. Emily A. Carter for their help and useful discussion throughout this work.

■ REFERENCES

(1) Swenson, H.; Stadie, N. P. Langmuir's Theory of Adsorption: A Centennial Review. *Langmuir* **2019**, *35* (16), 5409−5426.

(2) Langmuir, I. THE ADSORPTION OF GASES ON PLANE SURFACES OF GLASS, MICA AND PLATINUM. *J. Am. Chem. Soc.* **1918**, *40* (9), 1361−1403.

(3) Frumkin, A. Die Kapillarkurve der höheren Fettsäuren und die Zustandsgleichung der Oberflächenschicht. *Zeitschrift für Physikalische Chemie* **1925**, *116U* (1), 466−484.

(4) Shockley, W. On the Surface States Associated with a Periodic Potential. *Phys. Rev* **1939**, *56* (4), 317−323.

(5) Friedel, J. Metallic alloys. *Nuovo Cim.* **1958**, *7* (2), 287−311.

(6) Lau, K. H.; Kohn, W. Indirect long-range oscillatory interaction between adsorbed atoms. *Surf. Sci.* **1978**, *75* (1), 69−85.

(7) Lau, K. H.; Kohn, W. Elastic interaction of two atoms adsorbed on a solid surface. *Surf. Sci.* **1977**, *65* (2), 607−618.

(8) Knorr, N.; Brune, H.; Epple, M.; Hirstein, A.; Schneider, M. A.; Kern, K. Long-range adsorbate interactions mediated by a two-dimensional electron gas. *Phys. Rev. B* **2002**, *65* (11), 115420.

(9) Kessler, J.; Thieme, F. Chemisorption of CO on differently prepared Cu(111) surfaces. *Surf. Sci.* **1977**, *67* (2), 405−415.

(10) Ertl, G.; Koch, J. Adsorption von CO auf einer Palladium(111)-Oberfläche. *Zeitschrift für Naturforschung A* **1970**, *25* (12), 1906−1912.

(11) Truong, C. M.; Rodriguez, J.; Goodman, D. W. CO adsorption isotherms on Cu(100) at elevated pressures and temperatures using infrared reflection absorption spectroscopy. *Surf. Sci.* **1992**, *271* (3), L385−L391.

(12) McElhiney, G.; Papp, H.; Pritchard, J. The adsorption of Xe and CO on Ag(111). *Surf. Sci.* **1976**, *54* (3), 617−634.

(13) Yang, H. J.; Minato, T.; Kawai, M.; Kim, Y. STM Investigation of CO Ordering on Pt(111): From an Isolated Molecule to High-Coverage Superstructures. *J. Phys. Chem. C* **2013**, *117* (32), 16429−16437.

(14) Zhang, D.; Virchenko, V.; Jansen, C.; Groot, I. M. N.; Juurlink, L. B. F. Adsorption Sites in the High-Coverage Limit of CO on Cu(111). *J. Phys. Chem. C* **2025**, *129* (7), 3493−3497.

(15) Eren, B.; Zherebetskyy, D.; Patera, L. L.; Wu, C. H.; Bluhm, H.; Africh, C.; Wang, L.-W.; Somorjai, G. A.; Salmeron, M. Activation of Cu(111) surface by decomposition into nanoclusters driven by CO adsorption. *Science* **2016**, *351* (6272), 475−478.

(16) Hammer, B.; Nørskov, J. K. Electronic factors determining the reactivity of metal surfaces. *Surf. Sci.* **1995**, *343* (3), 211−220.

(17) Chen, P.; Fan, D.; Zhang, Y.; Selloni, A.; Carter, E. A.; Arnold, C. B.; Dankworth, D. C.; Rucker, S. P.; Chelikowsky, J. R.; Yao, N. Breaking a dative bond with mechanical forces. *Nature Commun.* **2021**, *12* (1), 5635.

(18) Gross, L.; Moll, N.; Mohn, F.; Curioni, A.; Meyer, G.; Hanke, F.; Persson, M. High-Resolution Molecular Orbital Imaging Using a *p*-Wave STM Tip. *Phys. Rev. Lett.* **2011**, *107* (8), 086101.

(19) Fan, J.; Li, R.; Zhang, C. H.; Zou, H. *Statistical Foundations of Data Science*. CRC Press, 2020; p 774.

(20) Devore, J. L. *Probability and Statistics for Engineering and the Sciences. Thomson/Brooks/Cole*; Cengage Learning, 2008.

(21) Liu, G.; Shih, A. J.; Deng, H.; Ojha, K.; Chen, X.; Luo, M.; McCrum, I. T.; Koper, M. T. M.; Greeley, J.; Zeng, Z. Site-specific reactivity of stepped Pt surfaces driven by stress release. *Nature* **2024**, *626* (8001), 1005−1010.

(22) Wahlström, E.; Ekvall, I.; Olin, H.; Walldén, L. Long-range interaction between adatoms at the Cu(111) surface imaged by scanning tunnelling microscopy. *Appl. Phys. A: Mater. Sci. Process.* **1998**, *66* (1), 1107−1110.

(23) Lewis, C. D. *Industrial and Business Forecasting Methods: A Practical Guide to Exponential Smoothing and Curve Fitting*. Butterworth Scientific, 1982.

(24) Chelikowsky, J. R.; Troullier, N.; Saad, Y. Finite-difference-pseudopotential method: Electronic structure calculations without a basis. *Phys. Rev. Lett.* **1994**, *72* (8), 1240−1243.

(25) Xu, L.; Lin, J.; Bai, Y.; Mavrikakis, M. Atomic and Molecular Adsorption on Cu(111). *Top. Catal.* **2018**, *61* (9), 736−750.

(26) Patra, A.; Peng, H.; Sun, J.; Perdew, J. P. Rethinking CO adsorption on transition-metal surfaces: Effect of density-driven self-interaction errors. *Phys. Rev. B* **2019**, *100* (3), 035442.

(27) Chen, Z.; Liu, Z.; Xu, X. Accurate descriptions of molecule-surface interactions in electrocatalytic CO2 reduction on the copper surfaces. *Nature Commun.* **2023**, *14* (1), 936.

(28) Stroppa, A.; Termentzidis, K.; Paier, J.; Kresse, G.; Hafner, J. CO adsorption on metal surfaces: A hybrid functional study with plane-wave basis set. *Phys. Rev. B* **2007**, *76* (19), 195440.

(29) Wellendorff, J.; Silbaugh, T. L.; Garcia-Pintos, D.; Nørskov, J. K.; Bligaard, T.; Studt, F.; Campbell, C. T. A benchmark database for adsorption bond energies to transition metal surfaces and comparison to selected DFT functionals. *Surf. Sci.* **2015**, *640*, 36−44.

(30) Perdew, J. P.; Chevary, J. A.; Vosko, S. H.; Jackson, K. A.; Pederson, M. R.; Singh, D. J.; Fiolhais, C. Atoms, molecules, solids, and surfaces: Applications of the generalized gradient approximation for exchange and correlation. *Phys. Rev. B* **1992**, *46* (11), 6671−6687.

(31) Kohn, W.; Sham, L. J. Self-Consistent Equations Including Exchange and Correlation Effects. *Phys. Rev.* **1965**, *140* (4A), A1133−A1138.

(32) Perdew, J. P.; Ruzsinszky, A.; Csonka, G. I.; Vydrov, O. A.; Scuseria, G. E.; Constantin, L. A.; Zhou, X.; Burke, K. Restoring the Density-Gradient Expansion for Exchange in Solids and Surfaces. *Phys. Rev. Lett.* **2008**, *100* (13), 136406.

(33) Perdew, J. P.; Burke, K.; Ernzerhof, M. Generalized Gradient Approximation Made Simple. *Phys. Rev. Lett.* **1996**, *77* (18), 3865−3868.

(34) Sun, J.; Ruzsinszky, A.; Perdew, J. P. Strongly Constrained and Appropriately Normed Semilocal Density Functional. *Phys. Rev. Lett.* **2015**, *115* (3), 036402.
(35) Zhang, Y.; Xu, X.; Goddard, W. A. Doubly hybrid density functional for accurate descriptions of nonbond interactions, thermochemistry, and thermochemical kinetics. *Proc. Natl. Acad. Sci.* **2009**, *106* (13), 4963−4968.
(36) Adamo, C.; Barone, V. Toward reliable density functional methods without adjustable parameters: The PBE0 model. *J. Chem. Phys.* **1999**, *110* (13), 6158−6170.
(37) Hammer, B.; Hansen, L. B.; Nørskov, J. K. Improved adsorption energetics within density-functional theory using revised Perdew-Burke-Ernzerhof functionals. *Phys. Rev. B* **1999**, *59* (11), 7413−7421.
(38) Wellendorff, J.; Lundgaard, K. T.; Møgelhøj, A.; Petzold, V.; Landis, D. D.; Nørskov, J. K.; Bligaard, T.; Jacobsen, K. W. Density functionals for surface science: Exchange-correlation model development with Bayesian error estimation. *Phys. Rev. B* **2012**, *85* (23), 235149.
(39) Vollmer, S.; Witte, G.; Wöll, C. Determination of Site Specific Adsorption Energies of CO on Copper. *Catal. Lett.* **2001**, *77* (1), 97−101.
(40) Becke, A. D. Density-functional thermochemistry. III. The role of exact exchange. *J. Chem. Phys.* **1993**, *98* (7), 5648−5652.
(41) Heyd, J.; Scuseria, G. E.; Ernzerhof, M. Hybrid functionals based on a screened Coulomb potential. *J. Chem. Phys.* **2003**, *118* (18), 8207−8215.
(42) Grimme, S.; Antony, J.; Ehrlich, S.; Krieg, H. A consistent and accurate ab initio parametrization of density functional dispersion correction (DFT-D) for the 94 elements H-Pu. *J. Chem. Phys.* **2010**, *132* (15), 154104.
(43) Comanici, K.; Buchner, F.; Flechtner, K.; Lukasczyk, T.; Gottfried, J. M.; Steinrück, H.-P.; Marbach, H. Understanding the Contrast Mechanism in Scanning Tunneling Microscopy (STM) Images of an Intermixed Tetraphenylporphyrin Layer on Ag(111). *Langmuir* **2008**, *24* (5), 1897−1901.
(44) Gameel, K. M.; Sharafeldin, I. M.; Abourayya, A. U.; Biby, A. H.; Allam, N. K. Unveiling CO adsorption on Cu surfaces: New insights from molecular orbital principles. *Phys. Chem. Chem. Phys.* **2018**, *20* (40), 25892−25900.
(45) Sharifzadeh, S.; Huang, P.; Carter, E. Embedded Configuration Interaction Description of CO on Cu(111): Resolution of the Site Preference Conundrum. *J. Phys. Chem. C* **2008**, *112* (12), 4649−4657.
(46) Nørskov, J. K.; Abild-Pedersen, F.; Studt, F.; Bligaard, T. Density functional theory in surface chemistry and catalysis. *Proc. Natl. Acad. Sci.* **2011**, *108* (3), 937−943.
(47) Nørskov, J. K. Chapter 1 - Adsorbate-adsorbate interactions on metal surfaces. In *The Chemical Physics of Solid Surfaces*. Elsevier, 1993, Vol. 6, pp. 1−27. .
(48) Silber, D.; Kowalski, P. M.; Traeger, F.; Buchholz, M.; Bebensee, F.; Meyer, B.; Wöll, C. Adsorbate-induced lifting of substrate relaxation is a general mechanism governing titania surface chemistry. *Nature Commun.* **2016**, *7* (1), 12888.
(49) Libuda, J.; Freund, H. J. Molecular beam experiments on model catalysts. *Surf. Sci. Rep.* **2005**, *57* (7), 157−298.
(50) Freund, H.-J. Model Studies in Heterogeneous Catalysis. *Chem. - Eur. J* **2010**, *16* (31), 9384−9397.
(51) Besenbacher, F.; Lauritsen, J. V.; Wendt, S. STM studies of model catalysts. *Nano Today* **2007**, *2* (4), 30−39.
(52) Wang, Y.; Liu, S.; Qin, Y.; Zhao, Y.; Liu, L.; Zhang, D.; Liu, J.; Liu, Y.; Chu, A.; Wu, H.; Jia, B.; Qu, X.; Li, H.; Qin, M. Chromium Promotes Phase Transformation to Active Oxyhydroxide for Efficient Oxygen Evolution. *ACS Catal.* **2024**, *14* (18), 13759−13767.
(53) Hansen, S. I.; Sjølin, B. H.; Castelli, I. E.; Vegge, T.; Jensen, A. D.; Christensen, J. M. An Adsorption Isotherm That Includes the Interactions between Adsorbates. *J. Phys. Chem. C* **2025**, *129* (11), 5393−5407.

https://doi.org/10.1021/jacs.5c13663
J. Am. Chem. Soc. 2026, 148, 360−367